

A 2m-Range 711 μ W Body Channel Communication Transceiver Featuring Dynamically-Sampling Bias-Free Interface Front End

Gu, Guanjie; Yang, Changgui; Zhao, Jian; Du, Sijun; Luo, Yuxuan; Zhao, Bo

DOI

[10.1109/TBCAS.2024.3439619](https://doi.org/10.1109/TBCAS.2024.3439619)

Publication date

2024

Document Version

Final published version

Published in

IEEE transactions on biomedical circuits and systems

Citation (APA)

Gu, G., Yang, C., Zhao, J., Du, S., Luo, Y., & Zhao, B. (2024). A 2m-Range 711 μ W Body Channel Communication Transceiver Featuring Dynamically-Sampling Bias-Free Interface Front End. *IEEE transactions on biomedical circuits and systems*, 19(2), 393-403.
<https://doi.org/10.1109/TBCAS.2024.3439619>

Important note

To cite this publication, please use the final published version (if applicable).
Please check the document version above.

Copyright

Other than for strictly personal use, it is not permitted to download, forward or distribute the text or part of it, without the consent of the author(s) and/or copyright holder(s), unless the work is under an open content license such as Creative Commons.

Takedown policy

Please contact us and provide details if you believe this document breaches copyrights.
We will remove access to the work immediately and investigate your claim.







Green Open Access added to TU Delft Institutional Repository

'You share, we take care!' - Taverne project

<https://www.openaccess.nl/en/you-share-we-take-care>

Otherwise as indicated in the copyright section: the publisher is the copyright holder of this work and the author uses the Dutch legislation to make this work public.

A 2m-Range 711 μ W Body Channel Communication Transceiver Featuring Dynamically-Sampling Bias-Free Interface Front End

Guanjie Gu , *Student Member, IEEE*, Changgui Yang , *Student Member, IEEE*,
Jian Zhao , *Senior Member, IEEE*, Sijun Du , *Senior Member, IEEE*, Yuxuan Luo , *Senior Member, IEEE*,
and Bo Zhao , *Senior Member, IEEE*

Abstract—Body Channel Communication (BCC) utilizes the body surface as a low-loss signal transmission medium, reducing the power consumption of wireless wearable devices. However, the effective communication range on the human body is limited in the state-of-the-art BCC transceivers, where the signal loss between the body surface and the BCC receiver remains one of the main bottlenecks. To reduce the interface loss, a high input impedance is desired by the BCC receiver, but the DC-biasing circuits decrease the input impedance. In this work, a dynamically-sampling IFE is proposed to eliminate the DC voltage bias, resulting in a 90k Ω high input impedance and a 94dB RF–IF conversion gain to reduce the interface loss in long-range BCC applications. The BCC transceiver chip is fabricated in 55nm CMOS process, taking a die area of 0.123mm². Measured results show that the chip extends the BCC range to 2m for both the forward and backward paths, where the transmitter and receiver consume 711 μ W power in total.

Index Terms—Body channel communication (BCC), interface front end (IFE), communication range, low power, input impedance.

I. INTRODUCTION

BODY Channel Communication (BCC) has been validated to be a power-efficient scheme in the signal transmission of wireless body area network (WBAN) [1]. A WBAN node is based on a battery-powered wireless device to monitor and transfer the physiological signals, which requires a miniature

size and a long life time. As the most power-hungry submodule in a WBAN node, the transceiver becomes the main design bottleneck to reduce the system power. Traditional RF communication suffers from the loss induced by body shielding in wearables, which should be compensated by circuits with higher power consumption. BCC utilizes the body surface as the signal-transmission medium, providing a low-power solution for transceiver designs. There are two main advantages of BCC over traditional wireless communication: 1) the conductivity of human body reduces the power consumption, and 2) antenna-free communication helps to minimize the system size [2]. Therefore, the BCC transceiver is regarded as one of the best candidates in further WBAN systems [3], [4], [5], [6].

In the state of the arts, only the electro-quasi-static (EQS) mechanism based chips have achieved whole-body coverage for BCC transmission [7]. Nonetheless, the signal wavelength must be much longer than the body size in the EQS mechanism. As a result, the carrier frequency in EQS mechanism is limited to be less than 1MHz [8]. For low power consumption, the works [7], [8] adopted the envelope-detection-based receivers, where the sensitivity was optimized at a carrier-to-data ratio of 100, limiting the data rate to be less than 20kbps. Therefore, the communication range for a >50kbps data rate is limited to <1m in the state of the arts [9]. For example, the BCC transceiver in [10] realized 1.4mW power and 2.5nJ/bit energy efficiency, while the communication range was less than 30cm. In addition, the effective communication range was extended to 1m in [11], at the penalty of 2.35mW power consumption. Moreover, the measurement in [12] showed that the bit error rate (BER) increased from 10^{−7} at a 5cm communication range to 10^{−2} at a 1m range, consuming 1.97mW power. As a result, the limited communication range of conventional BCC transceivers restricted the applicability in a number of WBAN scenarios, such as the signal transmission from a foot to a smartwatch [13].

One of the main factors limiting the effective communication range is the signal loss at the interface between the body surface and the BCC receiver. Relative to the high impedance of human body [14], a lower input impedance of the BCC receiver leads to significant signal attenuation. For the channel loss in the backward path [15], the backward coupling capacitance tends to be constant versus a long distance, while the value becomes

Manuscript received 17 March 2024; revised 9 May 2024 and 1 July 2024; accepted 22 July 2024. Date of publication 7 August 2024; date of current version 2 April 2025. This work was supported in part by the National Key R&D Program of China under Grant 2019YFB2204500, in part by the National Natural Science Foundation of China under Grant 61974130, and in part by “Chenguang Program” supported by Shanghai Education Development Foundation and Shanghai Municipal Education Commission. This paper was recommended by Associate Editor H. Jiang. (*Corresponding author: Bo Zhao.*)

Guanjie Gu, Changgui Yang, Yuxuan Luo, and Bo Zhao are with the College of Integrated Circuits, Zhejiang University, Hangzhou 310027, China (e-mail: zhaobo@zju.edu.cn).

Jian Zhao is with the Department of Micro/Nano Electronics, Shanghai Jiao Tong University, Shanghai 200240, China (e-mail: zhaojianycc@sjtu.edu.cn).

Sijun Du is with the Department of Microelectronics, Delft University of Technology, 2628 CD Delft, The Netherlands (e-mail: sijun.du@tudelft.nl).

Color versions of one or more figures in this article are available at <https://doi.org/10.1109/TBCAS.2024.3439619>.

Digital Object Identifier 10.1109/TBCAS.2024.3439619

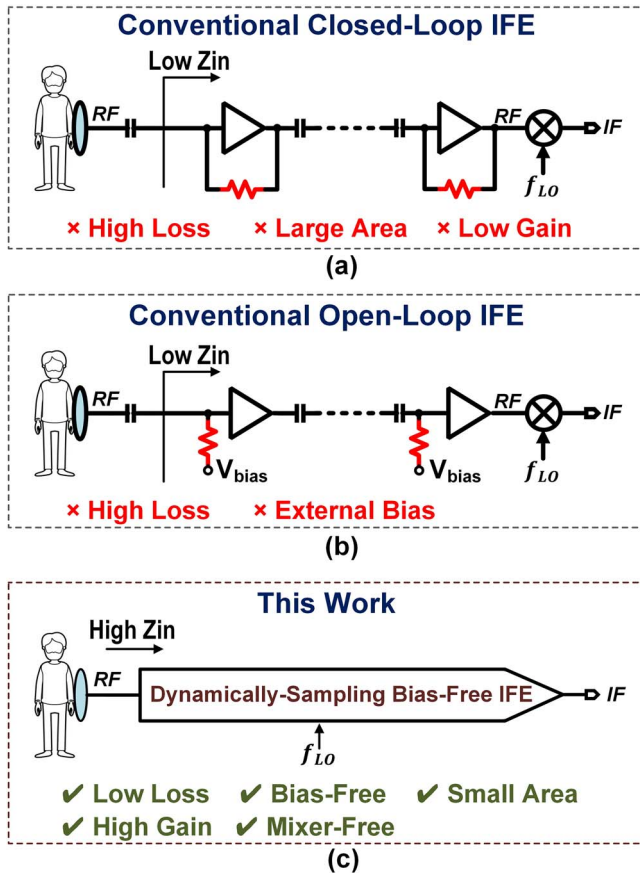


Fig. 1. Conventional interface front ends (IFE) of BCC transceivers and this work.

very small (usually less than 0.5pF), leading to a significant backward path loss. However, the small and constant backward coupling capacitance in the long distance can be canceled by a passive inductor [16] or an active component [17]. In long-distance transmission scenarios, the capacitance between the GND plane and earth ground induces much less impact on BCC transmission than backward capacitance. As a result, the interface loss between the human body and the receiver dominates the overall signal loss in BCC. Relative to the high impedance of human body [14], a lower input impedance of the BCC receiver leads to significant signal attenuation on the body-receiver interface. Therefore, an interface front end (IFE) of a BCC receiver should be designed with a high input impedance and a high gain to reduce the interface loss. There were two conventional typologies to implement the IFE of BCC receivers, as shown in Fig. 1:

- 1) Closed-loop IFE. Negative feedback was adopted to provide self-biasing DC voltages for cascaded IFE stages, as shown in Fig. 1(a). A feedback resistor is needed to establish the DC operating point. Compared to the high impedance of the MOSFET gate terminal, the feedback resistor decreases the overall input impedance and gain of the IFE, which leads to a voltage loss at the body-receiver interface. For example, the interface amplifier with negative feedback resulted in a gain of 20dB, achieving a

communication range of 15cm with 5mW power [4]. The communication range was extended to 1m in [18] by a receiver with 10k Ω input impedance, which was at the penalty of 9mW power consumption.

- 2) Open-Loop IFE with external DC bias. The IFE presents an open-loop structure without feedback, where the input stage can be the gate terminal of a MOSFET [19], [20], providing a higher impedance and a higher voltage gain than the closed-loop structure. However, a biasing resistor connects the MOSFET gate terminal to a voltage reference, which degrades the high input impedance of the MOSFET gate terminal. Thus, there is a voltage loss at the body-receiver interface. For example, the open-loop IFE in [19] realized 1k Ω input impedance and -62dB sensitivity of BCC receiver. As a result, the BCC transceiver with 6.44mW power consumption achieved a communication range of 20cm [20]. Compared to poly-resistor biasing, the pseudo-resistor biasing [21] takes a smaller chip area. However, additional circuits such as voltage references are required, which increase the power consumption and noise.

Subsequent to the IFE, a mixer is also needed for downconversion in both conventional structures, which enlarges the die area and power consumption of BCC transceivers.

In this work, we propose a dynamically-sampling technique to realize a bias-free IFE, which helps the BCC receiver to achieve a high input impedance of 90k Ω . and a high RF–IF gain of 94 dB. In this way, the interface loss between the body surface and the BCC receiver is reduced from 84dB to 55dB, which improves the receiving sensitivity. In addition, the high input impedance and high gain of the proposed IFE can reduce the stage number and minimize the AC-coupling capacitors. The proposed technique is implemented in a BCC transceiver chip fabricated in 55nm CMOS process. Measured results show that the BCC transceiver achieves a communication range of 2m, at a BER of 2×10^{-4} . In this case, the BCC transmitter (TX) and receiver (RX) only consume 711 μ W in total.

The rest of this paper is organized as follows. Section II describes the proposed dynamically-sampling IFE technique. The system architecture of BCC transceiver is presented in Section III, and the measurement results are given in Section IV. Finally, Section V concludes the paper.

II. DYNAMICALLY-SAMPLING INTERFACE FRONT END

A. Modeling and Measurement of Body Channel

For BCC channel measurement, a standard setup is widely adopted in previous BCC works, while different cases (such as different distances, frequencies, electrodes, GND planes, etc) result in diverse results. For example, the setup in research [22] focused on the channel loss at operating frequencies below 1MHz. In the <1MHz frequency band, the propagation loss is relatively low and constant versus the distance due to the long wavelength, but the data rate can only be 1–20kbps. In addition, the setup in reference [23] focuses on studying the influence of GND electrodes. In this work, we study the path loss in

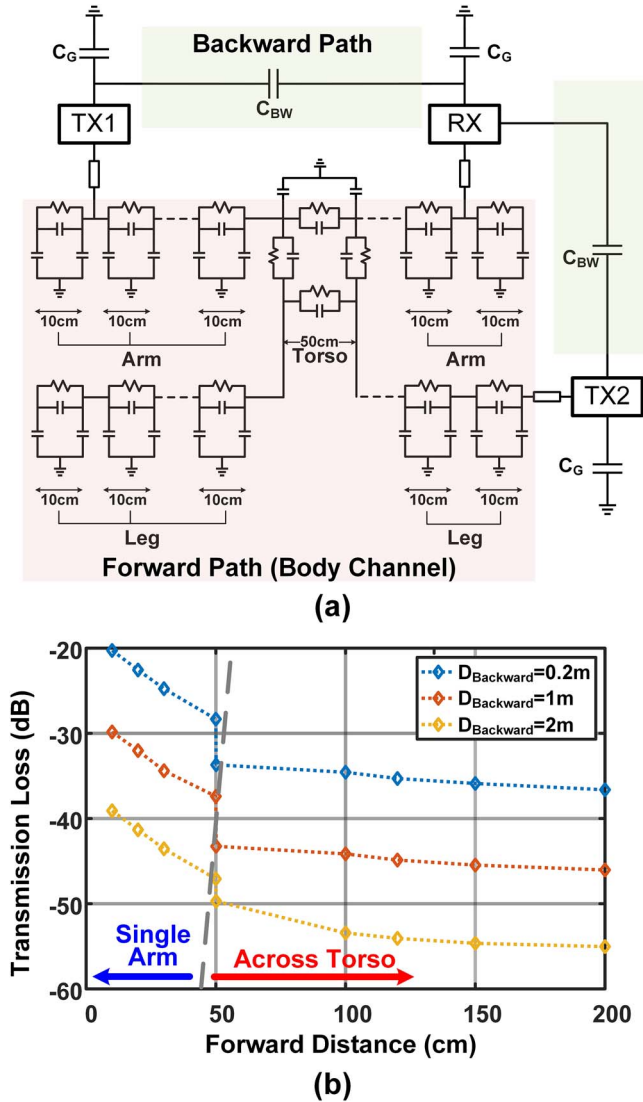


Fig. 2. (a) Circuit model of body channel. (b) Simulated transmission loss versus forward & backward distances ($D_{Backward}$).

long-range BCC at the operating frequency of 16–24MHz, to realize a communication data rate of 500kbps.

A five-tissue-layer channel model of BCC is built to analyze the loss in long-range human body signal transmission, which is explored from our previous work in [24], [25]. The circuit model is shown in Fig. 2, where a human body is mainly composed of arms, legs, and a torso. The circuits representing arms and legs are divided into a series of 10cm segments, where each unit is equivalent to an RC network. In addition, the torso is modeled by a 50cm-diameter cylinder composed of an RC network. The signal-transmission channel consists of a forward path on the body surface, as well as a backward path formed by the capacitive coupling (C_{BW}) between the ground planes of TX and RX. Moreover, both the ground planes also induce parasitic capacitance (C_G) over the external ground. Through the circuit model, the channel loss of BCC can be simulated and analyzed at different communication ranges along with the channel impedance and RX impedance.

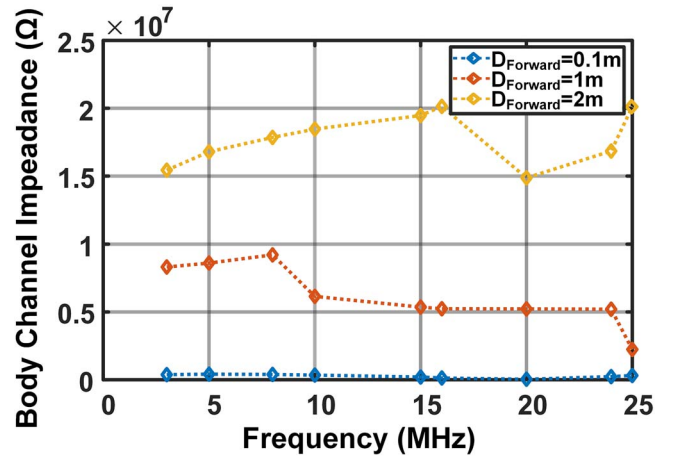


Fig. 3. Measurement results of forward body channel impedance ($D_{Forward}$: Forward distance).

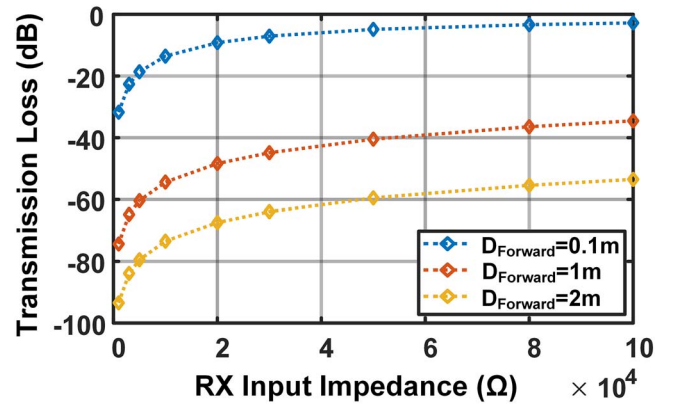


Fig. 4. Simulated transmission loss versus RX input impedance.

The impedance of TX–RX channel on the human body is studied by measurement. The signal loss at the interface is determined by the ratio of body-channel impedance over the receiver input impedance. Through a pair of electrodes on human body, the TX–RX channel impedance is measured in Fig. 3, which shows a channel impedance of 23.2k Ω to 16M Ω corresponding to a forward path length of 0.1m–2m. It can be seen that the channel impedance increases significantly versus the forward length. As a result, the interface loss versus the RX input impedance at 20MHz is given in Fig. 4. Targeting a long communication range on human body, the IFE must be designed with a high impedance to reduce the interface loss.

The simulation of overall channel loss at different communication ranges is based on both the circuit model and channel-impedance measurement. Fig. 2(b) illustrates the channel loss versus both forward and backward distances at 20MHz. For a short forward path on the arm (≤ 50 cm), the BCC shows a signal transmission loss of less than -30dB. At a long-range transmission, the signal is transferred across the torso, which leads to an abrupt increase in channel loss. For example, the signal transmission through a 2m range corresponds to -55dB channel loss, where -37dB loss appears at the interface between

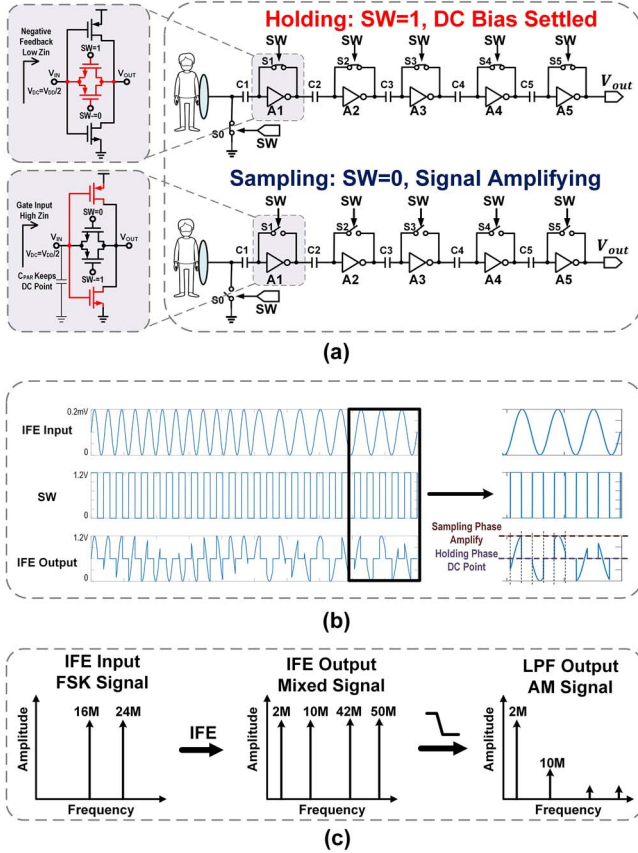


Fig. 5. Proposed interface front end (IFE): (a) Schematic, (b) time-domain waveforms, and (c) signal spectrums.

the human body and the BCC receiver. As a result, reducing the interface loss is essential to realize a long-range signal transmission in BCC, which requires both a high input impedance and a high gain of IFE.

B. Dynamically-Sampling Technique

A dynamically-sampling technique is proposed to increase both the input impedance and the voltage gain of the IFE in BCC receiver. The schematic of the proposed IFE is shown in Fig. 5, which is composed of high-gain inverter-based amplifiers with feedback switches. The switches are controlled by the SW signal, generated by a low-power phase-locked loop (PLL). The proposed IFE operates in a duty-cycled way composed of two phases, i.e., the holding phase and the sampling phase. In the holding phase, all the feedback switches are turned on, connecting the input and output of the inverter-based amplifier. The DC operating points are set by the feedback across the input and output terminals of the inverters. As the input and output of each stage is shorted, the strong feedback provides stable DC operating points versus PVT variations, and a sufficient phase margin is designed for each stage. In the sampling phase, all the feedback switches are shut down to configure the IFE as an open-loop amplifier chain. The biasing circuit is eliminated because the DC operating points of all the nodes are still maintained due to the parasitic capacitance. As the

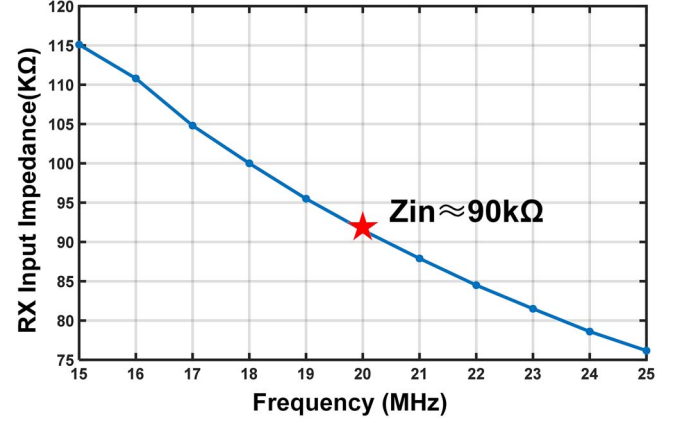


Fig. 6. Simulated input impedance of BCC RX.

TABLE I
COMPARISON WITH STATE-OF-THE-ART FRONT ENDS

	JSSC'20 [20]	JSSC'17 [10]	JSSC'19 [29]	JSSC'19 [30]	This Work
Frequency	40MHz	20-120MHz	21MHz	30-120MHz	16/24MHz
Gain	NA	15-27dB	29dB	10dB	94dB
Power	NA	NA	60μW	9μW	261μW
Bias	Ext	Ext	Ext	Ext	Self
Zin	10kΩ	100Ω	1kΩ	22kΩ	90kΩ

inverters amplify the input FSK signal limitedly into a rail-to-rail waveform, only the zero-crossing points of the waveform contain data information, while the distortion on the amplitude induced by the supply interferes induces little impact. In addition, the gate terminal of a MOSFET acts as the IFE input, resulting in a high input impedance of the BCC receiver. In this way, the channel loss can be significantly reduced by the high input impedance of the proposed IFE and the high gain, extending the communication range. To mitigate the impact of clock feedthrough, transmission gates are adopted as switches, which cancels the clock feedthrough by 17.5dB.

The input impedance and voltage gain of the proposed IFE are validated by simulation. In the sampling phase, the input impedance is simulated in Fig. 6 versus the carrier frequency. The gate input of IFE achieves a capacitive impedance higher than 90kΩ in the 16MHz–24MHz frequency band, reducing the signal loss at the body-RX interface. In addition, the proposed IFE achieves an RF-IF gain of 94dB across the FSK communication band, which helps to amplify the small received signal and compensate the loss at the interface. Table I shows the comparison with the state-of-the-art IFEs. For high-input-impedance designs in previous studies such as [20] and [30], the AC coupling and gate-input common-source amplifiers were adopted as the first stage, but both the two designs require external bias circuits. As a result, the input impedance is limited by the biasing resistors. In this work, the inverter-based amplifiers with switch-controlled negative feedback are adopted to eliminate the bias resistors. It can be seen that the proposed IFE achieves a higher input impedance and a higher gain compared to other IFEs, which helps to achieve a transmission distance of 2m.

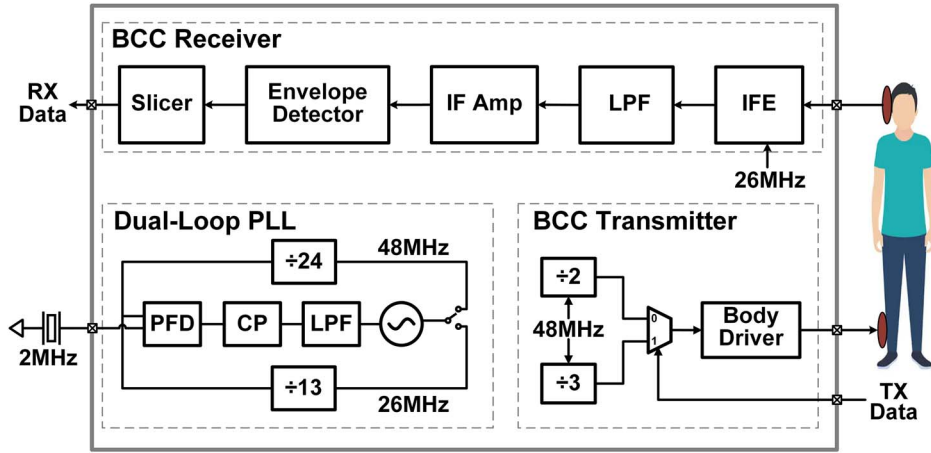


Fig. 7. BCC transceiver architecture.

The DC offset in the conventional high-gain RX front end can be eliminated by the proposed dynamically-sampling technique. Conventional RX front end increased the gain by multiple amplifying stages, where the DC offset was reduced by AC-coupling capacitors [26] or feedback cancellation [19]. Nevertheless, the low carrier frequency of BCC (e.g., ~ 21 MHz IEEE802.15.6 standard frequency [27]) induces a negative effect on the AC-coupling methods, whereas the feedback loops degrade the voltage gain. In the proposed IFE, the DC offsets in each stage are removed during the holding phase, when the feedback of inverters settles the DC points. As the signal amplification is conducted during the following sampling phase, the feedback formed in the holding phase will not decrease the IFE gain.

The dynamically-sampling operation down-converts the RF signals into an intermediate frequency (IF), eliminating the use of a mixer. In conventional IFEs, a mixer is required as the signal down-converter [10], which also needs biasing circuits. In this work, the signal is amplified and passed to the subsequent stages in the sampling phase, while the input signal is blocked during the holding phase, as given in Fig. 5. The on-off operation is equivalent to multiplying the input signal with a 0–1 rectangular waveform, performing the function of a sampling mixer. In this way, the 16 MHz–24 MHz FSK RF signal is sampled by a 26 MHz clock and then down-converted to an IF ranging in 2 MHz–10 MHz. While the upper-band components (10 MHz & 42 MHz–50 MHz tones) can be rejected by the subsequent LPF. Therefore, the IFE eliminates the use of a mixer and auxiliary circuits, reducing the chip area and power consumption.

III. SYSTEM ARCHITECTURE

The proposed IFE technique is implemented in a BFSK BCC transceiver, and the block diagram is shown in Fig. 7. The system clock is generated by a 2 MHz crystal oscillator and a dual-mode PLL, providing an FSK carrier signal for the transmitter as well as a sampling clock for the receiver. The FSK signal is formed in the transmitter, including two frequency dividers, a

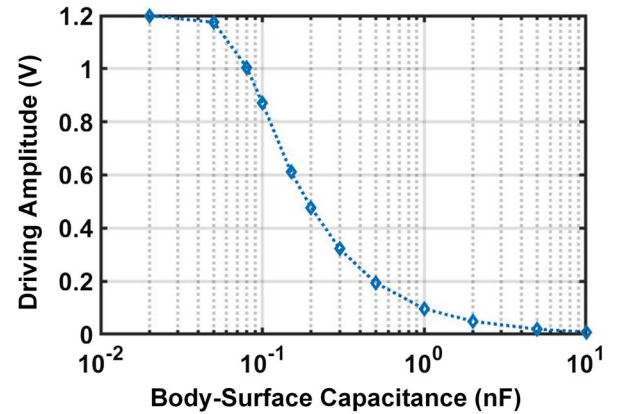


Fig. 8. Simulated transmitter driving ability.

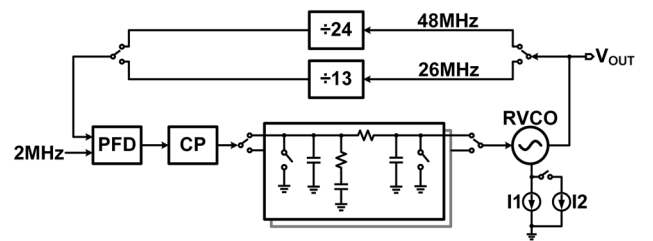


Fig. 9. Dual-mode integer-N PLL.

multiplexer (MUX), and a body driver. The BCC receiver is composed of the dynamically-sampling bias-free IFE, a 4th-order Sallen-Key LPF, an IF amplifier (IFA), an envelope detector, and a slicer. The baseband data can be modulated in the transmitter and then transmitted through the body surface. Meanwhile, the receiver picks up the signal from the human body, which was finally demodulated and recovered into a data stream.

The BCC transmitter is designed to generate a BFSK signal at a central frequency of 20 MHz. With a 48 MHz frequency output of PLL, a pair of $\div 2$ and $\div 3$ dividers are used to generate

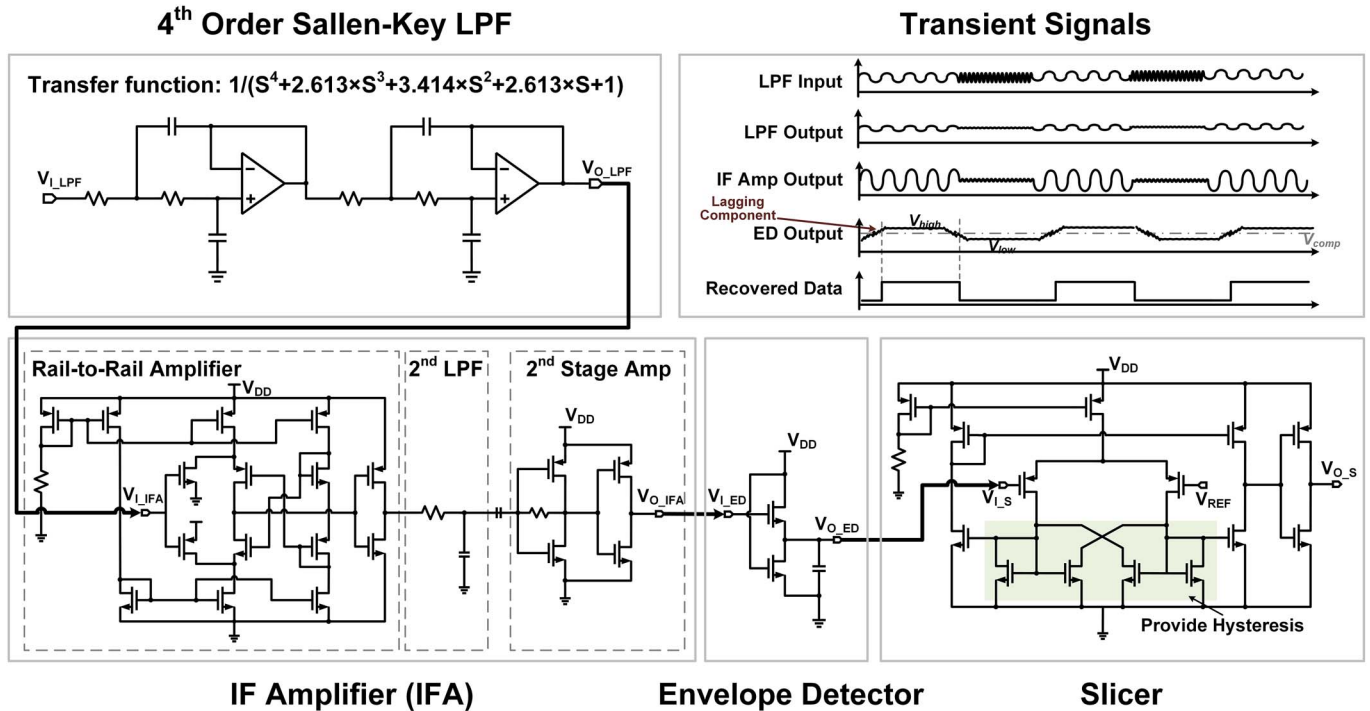


Fig. 10. Circuit details of LPF, IF amplifier (IFA), envelope detector, and slicer.

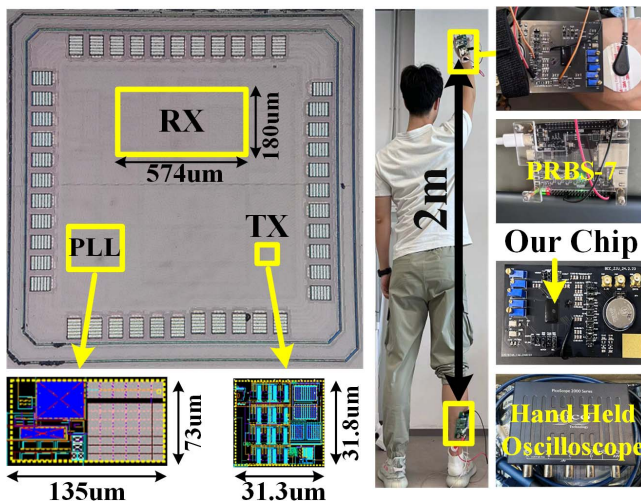


Fig. 11. Die micrograph and testing setup.

24MHz and 16MHz frequency components. The baseband data controls the MUX to switch between the two frequency components, resulting in a 16MHz–24MHz BFSK signal. Finally, a four-stage inverter-based body driver is designed to send the signal through the body surface, where the transistors in each stage are twice wider than in the previous stage. As shown in Fig. 8, the output voltage amplitude can reach a rail-to-rail output at a load capacitor of 80pF, ensuring the FSK signal to be effectively delivered to the human body. The TX benefits from a simple structure and low power.

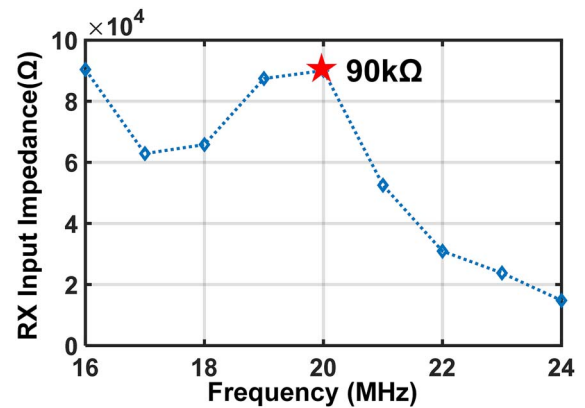


Fig. 12. Measured RX input impedance.

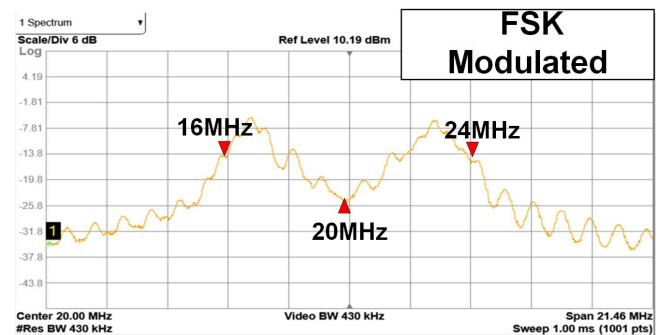


Fig. 13. Measured TX spectrum.

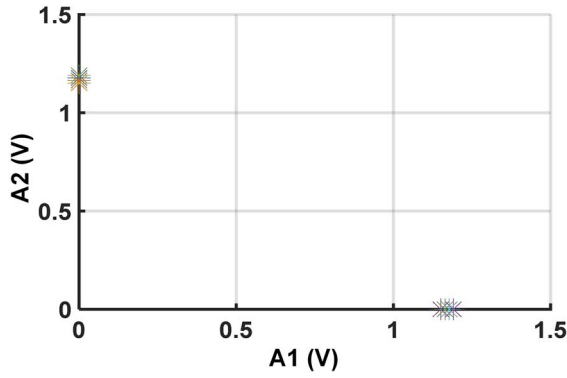


Fig. 14. Measured EVM of TX output.

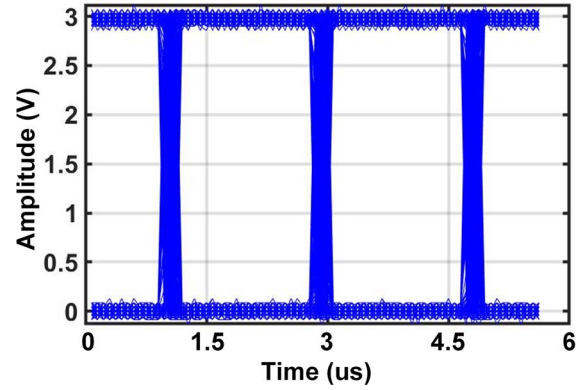


Fig. 16. Measured eye diagram.

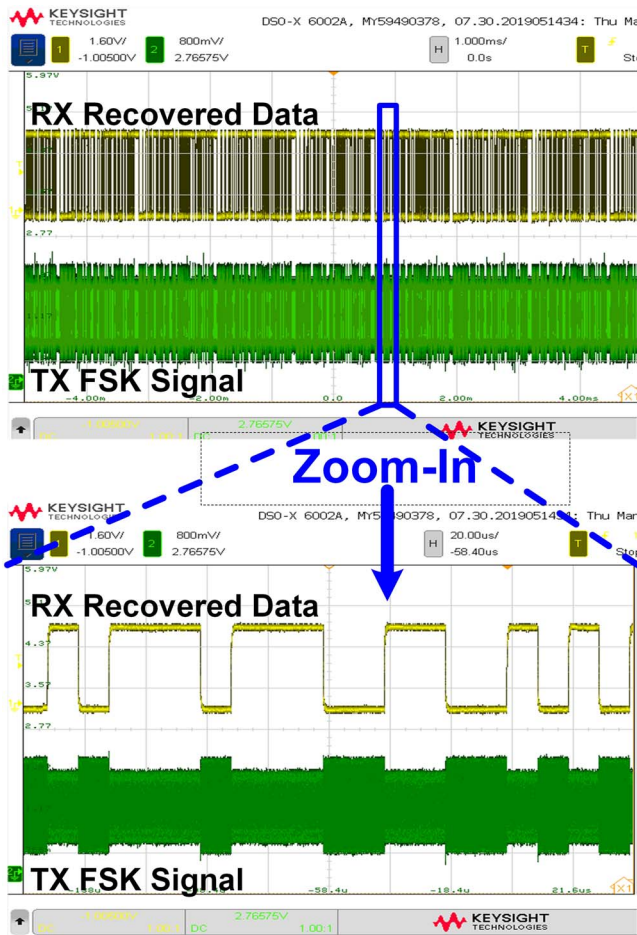


Fig. 15. Measured FSK signal transmitted by TX and recovered data by RX.

In the receiving mode, the BFSK signal is amplified and down-converted by the proposed IFE, providing a high gain to ensure a long communication range. After the down-converting, the IF signal presents 2MHz and 10MHz frequency components. Subsequently, the four-stage Sallen-Key LPF with 3MHz corner frequency is designed to suppress the 10MHz

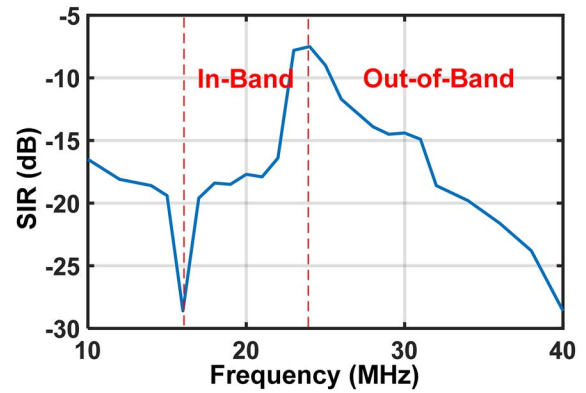


Fig. 17. Measured SIR performance of BCC receiver.

higher-frequency component while passing the 2MHz IF signal. As a result, the FSK signal is converted into an AM waveform, where the 2MHz component shows a much higher amplitude than the 10MHz one, corresponding to data 1 and 0, respectively. Afterward, an envelope detector is utilized to demodulate the AM signal, which is finally recovered into a '0-1' bit stream.

IV. CIRCUIT DETAILS

With a 2MHz crystal reference, the PLL is designed to generate the TX FSK frequencies as well as the RX sampling clock. The frequency divider in the PLL is set to 24 and 13 for the transmitting and receiving modes, respectively. In the transmitting mode, the PLL output a 48MHz frequency, which is utilized to generate the 16MHz and 24MHz FSK components by dividers and MUX. In the receiving mode, the PLL generates a 26MHz sampling clock for the IFE. As shown in Fig. 9, the two modes of PLL share most of the components except the divider and the loop filter to minimize the chip area. The loop filter switches between the transmitting and receiving modes, to ensure a 70° phase margin. A current-starve ring oscillator is adopted as the voltage-controlled oscillator (VCO) of PLL, which consumes 4 μ A and 7 μ A at the 26MHz receiving mode and 48MHz transmitting mode, respectively.

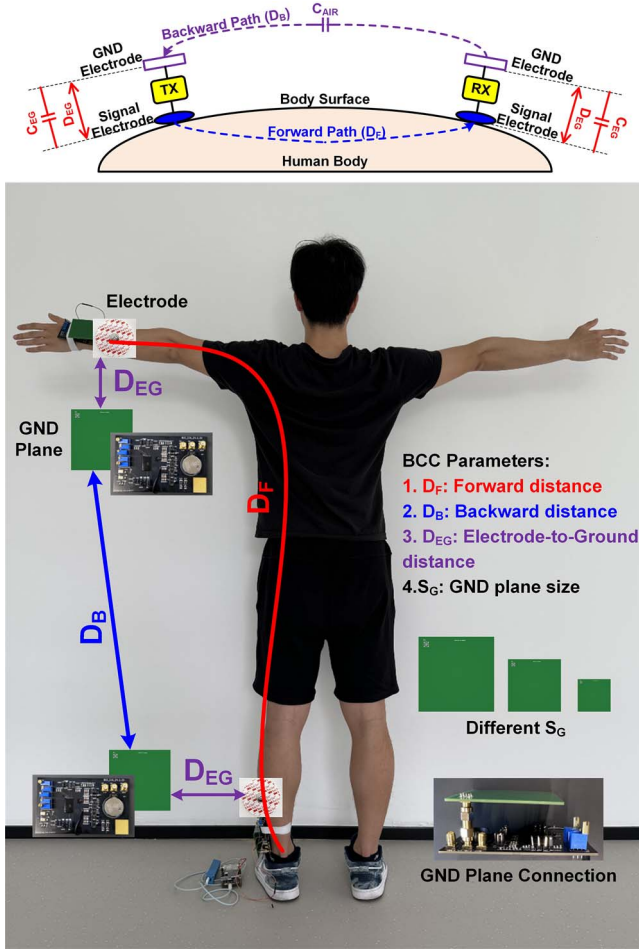


Fig. 18. Measured parameters of BCC transceiver at different forward distances, backward distances, electrode-to-ground distances, and ground plane sizes.

Subsequent to the IFE, the LPF suppresses the harmonics generated by the simple TX as well as the upper sideband output by the IFE. The schematic and transfer function of LPF is given in Fig. 10. The main design target of the IF filter is to pass the 2MHz signal while filtering out the 10MHz sideband and other higher-frequency components. As a result, the IF filter should reject the 10MHz components to be at least -40dB lower than the desired 2MHz signal. Therefore, a 4th-order Sallen-Key structure is selected to realize the -40dB rejection, which offers a quality factor of $Q=1.3$ and a passband gain of 0dB with minimal number of large capacitors, to save the die area.

The AM signal output by the 4th-order Sallen-Key LPF is amplified by an IFA. The amplitude of the AM signal ranges in 26mV–32mV, which is amplified into 800mV by the IFA, enabling the demodulation by the subsequent envelop detector. The schematic of IFA is given in Fig. 10, which includes a rail-to-rail input amplifier, a passive-RC filter, and a buffer. The rail-to-rail input amplifier adapts to a range of input signals, and then the passive-RC filter rejects the interference. As shown in Fig. 10, the envelop detector converts the AM signal into a data waveform. Finally, a slicer is adopted to recover the 0–1 bit

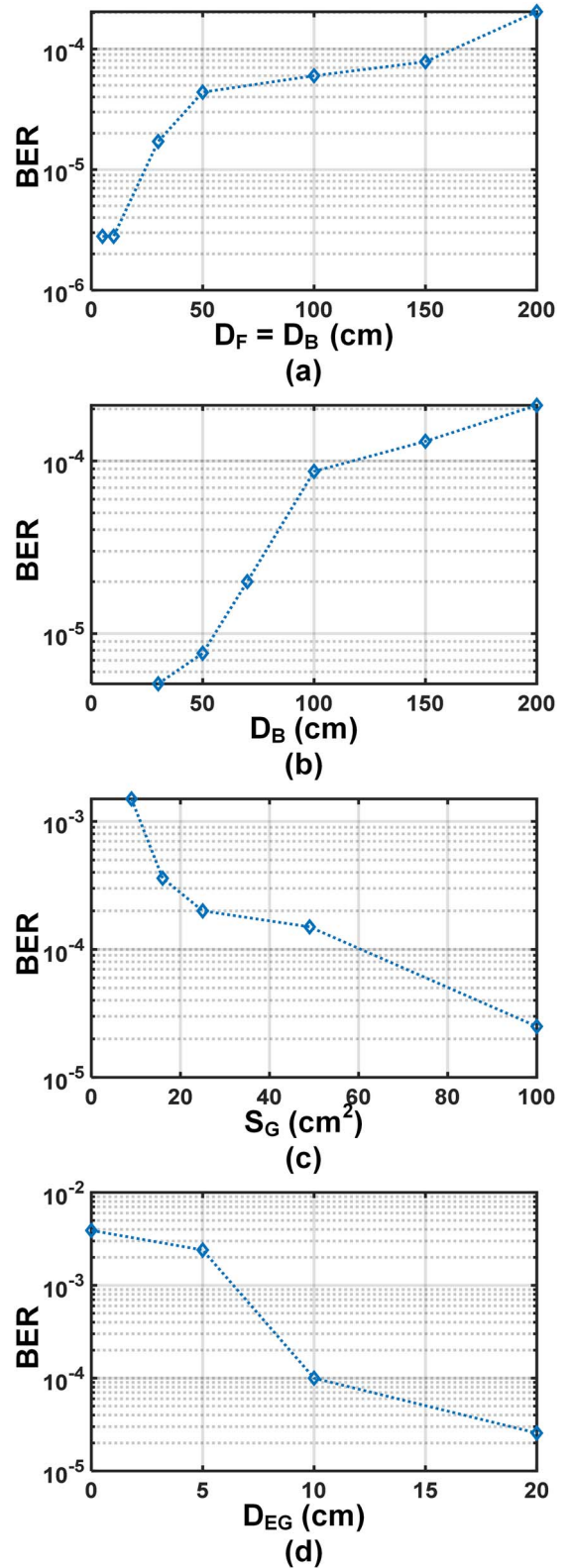


Fig. 19. Measured BER versus different parameters (D_F : Forward distance, D_B : Backward distance, S_G : ground size, and D_{EG} : Electrode-to-ground distance).

stream. The cross-coupled transistors provide a hysteresis to tolerate the interferers. The signal waveforms in the IF circuits are illustrated in Fig. 10.

TABLE II
PERFORMANCE COMPARISON

	JSSC'20 [20]	JSSC'17 [10]	JSSC'19 [28]	JSSC'19 [29]	JSSC'22 [7]	JSSC'19 [30]	TBCAS'23 [31]	JSSC'22 [9]	This Work
Process	180nm	65nm	65nm	65nm	65nm	65nm	180nm	28nm	55nm
Electrode	Ag/AgCl	Ag/AgCl	Gold	Ag/AgCl	Metal	Metal	Metal	Ag/AgCl	Ag/AgCl
RX Input	10k Ω	100 Ω	N/A	1k Ω	N/A	22k Ω	N/A	N/A	90kΩ
RX Sensitivity	-98.9dBm	-78dBm	-60dBm	-72dBm	-60dBm	-63.3dBm	N/A	N/A	-104dBm
Data Rate	240Kbps	1Mbps	80Mbps	5.25Mbps	1-20Kbps	30Mbps	10Mbps	0.1/27Mbps	500Kbps
BER	N/A	10^{-7}	10^{-5}	10^{-7}	10^{-5}	10^{-3}	10^{-3}	N/A	10^{-5} *
Crystal	21MHz	N/A	40MHz	42MHz	N/A	N/A	N/A	N/A	2MHz
Total Power	5.9mW	2.5mW	9.7mW	4.14mW	2.26uW	191uW	2.3mW	76uW	0.71mW
TX Power	0.9mW	1.1mW	1.7mW	3.52mW	2.19uW	93uW	1.125mW	76uW	0.214mW
RX Power	5mW	1.4mW	8mW	0.62mW	72nW	98uW	1.192mW	N/A	0.49mW
Core Area	14.44mm ²	2.13mm ²	16mm ²	0.672mm ²	0.056mm ²	N/A	0.216mm ²	0.0418mm ²	0.123mm ²
Energy/Bit	3.8nJ/bit	2.5nJ/bit	0.12nJ/bit	4.2nJ/bit	0.11nJ/bit	6.37pJ/bit	231.7pJ/bit	170/2.8pJ/bit	1.42nJ/bit
Range	20cm	30cm	20cm	N/A	F.B**	N/A	1m	50cm	2m

*The measured BER in this work presents to be 10^{-5} at 1m range and 10^{-4} at 2m range, respectively.

**F.B: Full body.

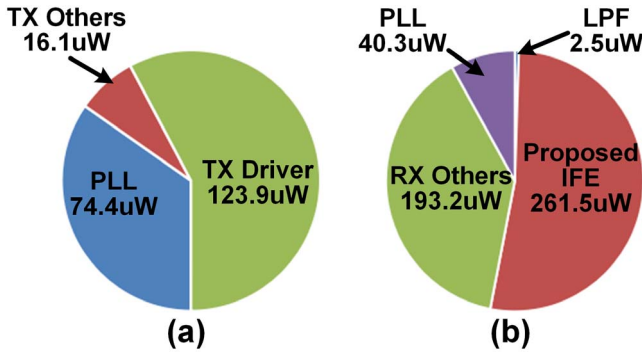


Fig. 20. Power breakdown.

V. EXPERIMENTAL RESULTS

The BCC transceiver chip is implemented in 55nm CMOS process, and Fig. 11 shows the die photo and measurement setup. The core circuit takes a total area of 0.123mm², including a 31 μ m \times 32 μ m TX, a 574 μ m \times 180 μ m RX, and a 135 μ m \times 73 μ m PLL. The maximum transmission ranges of both the forward path on the body surface and the backward path in capacitive coupling are set to 2m. A PRBS-7 bit stream is transferred through a 2m range (from the ankles to the wrist), where a pair of 3M medical electrodes are used as the contact between human body and BCC transceiver chips. To avoid signal transmission through the power line, both the BCC TX and RX are powered by a button battery. The PRBS-7 bit stream is produced by a waveform generator and the recovered data is collected by a hand-held oscilloscope.

As one of the key building blocks in the BCC transceiver chip, the proposed IFE is tested individually. The input

impedance of the proposed IFE versus the RX input frequency is measured in Fig. 12. The IFE shows a 90k Ω input impedance at the central frequency of the operating band. According to the measured TX-RX channel impedance in Fig. 4, the 90k Ω IFE reduces the interface loss to -55dB in a transmission range of 2m.

The FSK BCC transmitter shows its output spectrum in Fig. 13. The FSK signal takes a bandwidth of 9MHz at a central frequency of 20MHz. The EVM performance of BCC TX measured in Fig. 14, where the BFSK TX signal shows an EVM of -19 dB. The operating frequency results in a low loss in the forward path on body surface [14]. With a PRBS-7 bit stream input, the TX output signal in the time domain is given in Fig. 15. The RX picks up the signal and recovers into 0–1 data, which is compared to the original PRBS-7 bit stream to evaluate the BER performance. The eye diagram in Fig. 16 indicates the BCC receiver performs effectively at a transmission distance of 2m.

The signal-to-interference ratio (SIR) performance of BCC RX is measured in Fig. 17. For the in-band interference, the SIR can be less than -7.5dB in the frequency band of 23MHz–24MHz and -16 dB within the range of 16MHz–22MHz. For the out-of-band interference, the SIR reaches -9dB from 25MHz to 31MHz, and goes below -15dB at other frequencies.

The sensitivity and BER of the BCC receiver are tested with a 500kbps PRBS-7 data stream. It shows that the receiver achieves a sensitivity of 0.2mV (correspond to -104dBm) at a BER of 6×10^{-5} . Therefore, the 94dB RF–IF gain of the proposed IFE has improved the sensitivity of the BCC receiver.

The performance of BCC transceiver is tested at different forward distances(D_F), backward distances(D_B), ground

plane sizes(S_G), and electrode-to-ground distances(D_{EG}). The measurement setup on human body is shown in Fig. 18, and all the measured results are given in Fig. 19. Firstly, the forward path on the body surface is kept to be equal to the channel length of backward capacitive coupling. The measured BER versus the overall communication distance shows that the BCC transceiver chip achieves a BER of 2×10^{-4} at a 2m distance. Secondly, the forward path is set to 2m, and the BER changes from 5×10^{-5} to 2×10^{-4} at a backward channel length of 30cm–2m. Thirdly, the measured BER is reduced from 1.5×10^{-3} to 2×10^{-5} as the ground plane of BCC transceiver is enlarged from 9cm^2 to 100cm^2 . Finally, the distance between signal electrodes and the ground is changed from 0cm to 20cm. In this case, a smaller coupling capacitance establishes a higher impedance between signal electrode and GND electrode, resulting in a higher voltage drop on the BCC receiver. As a result, The BER drops from 4×10^{-3} to 2×10^{-5} at a communication distance of 2m. Therefore, the 2m range of the proposed BCC transceiver can cover the communication of various wearable devices on the whole human body.

The power breakdown of the BCC transceiver chip is shown in Fig. 20. In the transmitting mode, the chip consumes $214.4\mu\text{W}$ power, including $140\mu\text{W}$ in the MUX, dividers, and body driver, as well as $74.4\mu\text{W}$ in the PLL. In the receiving mode, the overall power consumption is $497.5\mu\text{W}$, which is composed of $457.2\mu\text{W}$ consumed by the receiver chain and $40.3\mu\text{W}$ consumed by PLL. As a complete BCC system, the TX and RX consume $711\mu\text{W}$ in total.

The measurement results are summarized and compared with the state-of-the-art BCC transceivers in Table II. It shows that: 1) Both the $90\text{k}\Omega$ high RX input impedance and the 94dB high gain of proposed IFE help the BCC receiver to achieve a 2m effective range with a data rate of 500kbps, which is the longest among the works with $>50\text{kbps}$ data rates. 2) The total power consumption of transmitting and receiving modes is reduced to $711\mu\text{W}$. 3) The proposed IFE technique achieves the best sensitivity due to the $90\text{k}\Omega$ high input impedance and 94dB RF–IF conversion gain.

VI. CONCLUSION

The state-of-the-art BCC transceivers have realized ultra-low power consumption, but the communication range for a $>50\text{kbps}$ data rate is limited to less than 1m. One of the issues limiting the communication range of BCC is the loss at the interface between human body and RX. The DC bias in previous self-biasing and gate-input techniques reduced the input impedance and voltage gain of IFE, leading to a high interface loss. In this work, we propose a dynamically-sampling bias-free IFE to realize a $90\text{k}\Omega$ input impedance and 94dB RF–IF gain of IFE, resulting in a receiving sensitivity of -104dBm . Therefore, the communication range has been extended to 2m with $711\mu\text{W}$ total power consumption. The proposed technique enables the BCC transceiver to cover the whole human body, such as the signal transmission from a foot to a smartwatch.

REFERENCES

- [1] Li, J., et al. "Body-coupled power transmission and energy harvesting." *Nature Electron.* vol. 4, pp. 530–538, Jul. 2021.
- [2] B. Zhao, J. Mao, J. Zhao, H. Yang, and Y. Lian, "The role and challenges of body channel communication in wearable flexible electronics," *IEEE Trans. Biomed. Circuits Syst.*, vol. 14, no. 2, pp. 283–296, Apr. 2020.
- [3] S. Maity, D. Yang, B. Chatterjee, and S. Sen, "A sub-nW wake-up receiver for human body communication," in *Proc. IEEE Biomed. Circuits Syst. Conf. (BioCAS)*, 2018, pp. 1–4.
- [4] S. Song, N. Cho, and H. Yoo, "A 0.2-mW 2-Mb/s digital transceiver based on wideband signaling for human body communications," *IEEE J. Solid-State Circuits*, vol. 42, no. 9, pp. 2021–2033, Sep. 2007.
- [5] J. Li, Y. Dong, L. Lin, J. S. Y. Tan, J. Y. Fong, and J. Yoo, "Concurrent body-coupled powering and communication ICs with a single electrode," *IEEE J. Solid-State Circuits*, vol. 59, no. 4, pp. 1006–1016, Apr. 2024.
- [6] C. Lee et al., "A miniaturized wireless neural implant with body-coupled power delivery and data transmission," *IEEE J. Solid-State Circuits*, vol. 57, no. 11, pp. 3212–3227, Nov. 2022.
- [7] N. Modak et al., "EQS Res-HBC: A 65-nm electro-quasistatic resonant 5–240 μW human whole-body powering and 2.19 μW communication SoC with automatic maximum resonant power tracking," *IEEE J. Solid-State Circuits*, vol. 57, no. 3, pp. 831–844, Mar. 2022.
- [8] S. Maity et al., "Sub- μW RCComm: 415-nW 1–10-kb/s physically and mathematically secure electro-quasi-static HBC node for authentication and medical applications," *IEEE J. Solid-State Circuits*, vol. 56, no. 3, pp. 788–802, Mar. 2021.
- [9] G. Tochou et al., "A Sub-100- μW 0.1-to-27-Mb/s pulse-based digital transmitter for the human intranet in 28-nm FD-SOI CMOS," *IEEE J. Solid-State Circuits*, vol. 57, no. 5, pp. 1409–1420, May 2022.
- [10] W. Saadeh, M. A. B. Altaf, H. Alsuradi, and J. Yoo, "A pseudo OFDM with miniaturized FSK demodulation body-coupled communication transceiver for binaural hearing aids in 65 nm CMOS," *IEEE J. Solid-State Circuits*, vol. 52, no. 3, pp. 757–768, Mar. 2017.
- [11] J.-H. Lee, K. Kim, M. Choi, J.-Y. Sim, H.-J. Park, and B. Kim, "A 16.6-pJ/b 150-Mb/s body channel communication transceiver with decision feedback equalization improving $> 200\%$ area efficiency," in *Proc. Symp. VLSI Circuits*, 2017, pp. C62–C63.
- [12] W. Saadeh, M. A. B. Altaf, H. Alsuradi, and J. Yoo, "A 1.1-mW ground effect-resilient body-coupled communication transceiver with pseudo OFDM for head and body area network," *IEEE J. Solid-State Circuits*, vol. 52, no. 10, pp. 2690–2702, Oct. 2017.
- [13] H. Lee et al., "A 5.5mW IEEE-802.15.6 wireless body-area-network standard transceiver for multichannel electro-acupuncture application," *Proc. IEEE Int. Solid-State Circuits Conf. (ISSCC) Dig. Tech. Papers*, 2013, pp. 452–453.
- [14] N. Cho, J. Yoo, S. Song, J. Lee, S. Jeon, and H. Yoo, "The human body characteristics as a signal transmission medium for intrabody communication," *IEEE Trans. Microw. Theory Techn.*, vol. 55, no. 5, pp. 1080–1086, May 2007.
- [15] J. Mao, B. Zhao, Y. Lian, and H. Yang, "The effects of GND electrodes in capacitive-coupling body channel communication," *Proc. IEEE Biomed. Circuits Syst. Conf. (BioCAS)*, 2015, pp. 1–4.
- [16] J. Bae, K. Song, H. Lee, H. Cho, and H.-J. Yoo, "A 0.24-nJ/b wireless body-area-network transceiver with scalable double-FSK modulation," *IEEE J. Solid-State Circuits*, vol. 47, no. 1, pp. 310–322, Jan. 2012.
- [17] J. Zhao et al., "An auto loss compensation system for capacitive-coupled body channel communication," *IEEE Trans. Biomed. Circuits Syst.*, vol. 13, no. 4, pp. 756–765, Aug. 2019.
- [18] J. Lee et al., "30.7 A 60Mb/s wideband BCC transceiver with 150pJ/b RX and 31pJ/b TX for emerging wearable applications," *IEEE Int. Solid-State Circuits Conf. (ISSCC) Dig. Tech. Papers*, 2014, pp. 498–499.
- [19] J. Bae and H. Yoo, "A 45 μW Injection-Locked FSK wake-up receiver with frequency-to-envelope conversion for crystal-less wireless body area network," *IEEE J. Solid-State Circuits*, vol. 50, no. 6, pp. 1351–1360, Jun. 2015.
- [20] J. Jang, J. Lee, H. Cho, J. Lee, and H.-J. Yoo, "Wireless body-area-network transceiver and low-power receiver with high application expandability," *IEEE J. Solid-State Circuits*, vol. 55, no. 10, pp. 2781–2789, Oct. 2020.
- [21] R. R. Harrison and C. Charles, "A low-power low-noise CMOS amplifier for neural recording applications," *IEEE J. Solid-State Circuits*, vol. 38, no. 6, pp. 958–965, Jun. 2003.
- [22] S. Maity, K. Mojabe, and S. Sen, "Characterization of human body forward path loss and variability effects in voltage-mode HBC," *IEEE Microw. Wireless Compon. Lett.*, vol. 28, no. 3, pp. 266–268, Mar. 2018.

- [23] J. Mao, H. Yang, and B. Zhao, "An investigation on ground electrodes of capacitive coupling human body communication," *IEEE Trans. Biomed. Circuits Syst.*, vol. 11, no. 4, pp. 910–919, Aug. 2017.
- [24] J. Mao, H. Yang, Y. Lian, and B. Zhao, "A five-tissue-layer human body communication circuit model tunable to individual characteristics," *IEEE Trans. Biomed. Circuits Syst.*, vol. 12, no. 2, pp. 303–312, Apr. 2018.
- [25] J. Mao, B. Zhao, Y. Lian, and H. Yang, "A 5-tissue-layer lumped-element based HBC circuit model compatible to IEEE802.15.6," in *Proc. IEEE Int. Symp. Circuits Syst. (ISCAS)*, Lisbon, Portugal, 2015, pp. 2632–2635.
- [26] H. Cho et al., "A 79 pJ/b 80 Mb/s full-duplex transceiver and a 42.5 μ W 100 kb/s super-regenerative transceiver for body channel communication," *IEEE J. Solid-State Circuits*, vol. 51, no. 1, pp. 310–317, Jan. 2016.
- [27] IEEE standard for local and metropolitan area networks—Part 15.6: Wireless body area networks (BAN), Standard 802.15.6-2012, Jun. 2013. [Online]. Available: <http://www.IEEE802.org/15/pub/TG6.html>
- [28] J. Jang et al., "A four-camera VGA-resolution capsule endoscope system with 80-Mb/s body channel communication transceiver and sub-centimeter range capsule localization," *IEEE J. Solid-State Circuits*, vol. 54, no. 2, pp. 538–549, Feb. 2019.
- [29] B. Zhao, Y. Lian, A. M. Niknejad, and C. H. Heng, "A Low-power compact IEEE 802.15.6 compatible human body communication transceiver with digital sigma-delta IIR mask shaping," *IEEE J. Solid-State Circuits*, vol. 54, no. 2, pp. 346–357, Feb. 2019.
- [30] S. Maity, B. Chatterjee, G. Chang, and S. Sen, "BodyWire: A 6.3-pJ/b 30-Mb/s -30-dB SIR-tolerant broadband interference-robust human body communication transceiver using time domain interference rejection," *IEEE J. Solid-State Circuits*, vol. 54, no. 10, pp. 2892–2906, Oct. 2019.
- [31] T. He et al., "A re-configurable body channel transceiver towards wearable and flexible biomedical sensor networks," in *IEEE Trans. Biomed. Circuits Syst.*, vol. 17, no. 5, pp. 1022–1034, Oct. 2023.



Guanjie Gu (Student Member, IEEE) received the B.S. degree from the College of Information Science and Electronic Engineering, Hangzhou, China, in 2020, where he is currently working toward the Ph.D. degree in electronic science and technology. His research interests include analog/mixed signal IC design, body area network communications, and ultra-low-power transceivers for IoT devices.



Changgui Yang (Student Member, IEEE) received the B.S. degree from the College of Information Science and Electronic Engineering, Hangzhou, China, in 2019, where he is currently working toward the Ph.D. degree in electronic science and technology. His research interests include analog/mixed-signal IC design, biomedical sensor interface, and wireless power/data transmission circuits design for implantable medical devices.



Jian Zhao (Senior Member, IEEE) received the Ph.D. degree from the School of Mechanical Engineering, Nanjing University of Science and Technology, Nanjing, China, in 2017. From 2012 to 2015, he was a Visiting Scholar with the VLSI and Signal Processing Lab, National University of Singapore. From 2017 to 2019, he joined the Department of Electronic Engineering, Tsinghua University, China, as a Postdoctor. Currently, he is an Associate Professor with the Department of Micro and Nano Electronics, Shanghai Jiao Tong University, Shanghai, China. He has authored and co-authored more than 70 technical papers and two book chapters. His research interests include biomedical electronics and bio-inspired circuits and systems. He has served on organization committee/technical program committee/review committee for many prestigious IEEE conferences, including IEEE International Symposium on Circuits and Systems, IEEE International Symposium on Integrated Circuits and Systems, IEEE International Conference on Artificial

Intelligence Circuits and Systems, IEEE International Conference on Integrated Circuits, Technologies and Applications, and IEEE Asia Pacific Conference on Circuits and Systems. He served/serves as an Associate Editor for IEEE TRANSACTIONS ON CIRCUITS AND SYSTEMS I: REGULAR PAPERS from 2020 to 2023 and IEEE TRANSACTIONS ON BIOMEDICAL CIRCUITS AND SYSTEMS from 2024.



and 2014. He was a Summer Engineer intern with Qualcomm Technology Inc., San Diego, CA, USA, in 2016. He was a Visiting Scholar with the Department of Microelectronics, Fudan University, Shanghai, China, in 2018. He was a Postdoctoral Researcher with Berkeley Wireless Research Center, Department of Electrical Engineering and Computer Sciences, University of California, Berkeley, CA, USA. Between 2018 and 2020. In 2020, he joined the Department of Microelectronics, Delft University of Technology, Delft, The Netherlands, where he is currently an Assistant Professor. His research interests include energy-efficient integrated circuits and systems, including power management integrated circuits, energy harvesting, wireless power transfer, and DC/DC converters used in Internet-of-Things wireless sensors, wearable electronics, biomedical devices, and microrobots.

Sijun Du (Senior Member, IEEE) received the First Class in B.Eng. degree in electrical engineering from the University Pierre and Marie Curie, Paris, France, in 2011, and a Distinction in M.Sc. degree in electrical and electronics engineering from Imperial College, London, U.K., in 2012. He received the Ph.D. degree in electrical engineering from the University of Cambridge, Cambridge, U.K., in 2018. He worked at the Laboratoire d'Informatique de Paris 6, University Pierre and Marie Curie and then worked as an IC Engineer in Shanghai, China, between 2012



Yuxuan Luo (Senior Member, IEEE) received the B.Eng. degree from the University of Electronic Science and Technology of China, Chengdu, China, in 2014, and the Ph.D. degree from the National University of Singapore, Singapore, in 2018. From 2018 to 2020, he worked as a Research Fellow with the National University of Singapore. Currently, he is a Tenure-Track Professor with the College of Integrated Circuits, Zhejiang University. His current research interest includes sensing circuits and systems. He serves as a Technical Program Committee

Member of the IEEE International Conference on Integrated Circuits, Technologies, and Applications (ICTA), the Tutorial Chair of ICTA 2024, the Sub-Track Chair of 2022 IEEE Asia Pacific Conference on Circuits and Systems and a Guest Editor of Frontiers in Nanotechnology. He was a recipient of the 2018 The Institution of Engineers, Singapore Prestigious Engineering Award.



Bo Zhao (Senior Member, IEEE) received the Ph.D. degree from the Department of Electronic Engineering, Tsinghua University, Beijing, China, in 2011. From 2013 to 2015, he was a Research Fellow with the National University of Singapore, Singapore. From 2015 to 2018, he was an Assistant Project Scientist with Berkeley Wireless Research Center, Department of Electrical Engineering and Computer Sciences, University of California at Berkeley, Berkeley, CA, USA. Since 2018, he has been a Professor with the Institute of VLSI Design, Zhejiang University, Hangzhou, China. He has authored or co-authored more than 70 articles and book chapters, and he holds more than 30 patents. His research interests include IoT radios, wireless power transfer, and wearable/implantable radios. He was a recipient of the 2017 IEEE TRANSACTIONS ON CIRCUITS AND SYSTEMS Darlington Best Paper Award and the Design Contest Award of the 2013 IEEE International Symposium on Low Power Electronics and Design. He serves as the TPC Member of IEEE International Solid-State Circuits Conference, as an Associate Editor for IEEE TRANSACTIONS ON BIOMEDICAL CIRCUITS AND SYSTEMS (2024–) and IEEE TRANSACTIONS ON CIRCUITS AND SYSTEMS I: REGULAR PAPERS (2020–2023, Best AE). He also serves as a Committee Member of IEEE/C/SM. He was the Publication Chair of the 2016 IEEE Biomedical Circuits and Systems Conference. He is elected to be the Chair Elect of Biomedical and Life Science Circuits and Systems Society.